J. Biophotonics **8**, No. 4, 332–346 (2015) / **DOI** 10.1002/jbio.201400138

Journal of BIOPHOTONICS

FULL ARTICLE

Ex vivo optical measurements of glucose diffusion kinetics in native and diabetic mouse skin

Daria K. Tuchina[*, 1, 2], *Rui Shi*[1], *Alexey N. Bashkatov*[2, 3], *Elina A. Genina*[2, 3], *Dan Zhu*[1], *Qingming Luo*[1], *and Valery V. Tuchin*[1, 2, 3]

[1] Britton Chance Center for Biomedical Photonics, Wuhan National Laboratory for Optoelectronics, Huazhong University of Science and Technology, Wuhan 430074, China
[2] Research-Educational Institute of Optics and Biophotonics, Saratov State University, Saratov 410012, Russia
[3] Interdisciplinary Laboratory of Biophotonics, Tomsk State University, Tomsk 634050, Russia

Received 21 November 2014, revised 21 January 2015, accepted 16 February 2015
Published online 12 March 2015

Key words: Skin, glucose, diffusion, glycation, diabetes mellitus, optical clearing

The aim of this study was to estimate the glucose diffusion coefficients *ex vivo* in skin of mice with diabetes induced *in vivo* by alloxan in comparison to non-diabetic mice. The temporal dependences of collimated transmittance of tissue samples immersed in glucose solutions were measured in the VIS-NIR spectral range to quantify the glucose diffusion/permeability coefficients and optical clearing efficiency of mouse skin. The average thickness of intact healthy and diabetic skin was 0.023 ± 0.006 cm and 0.019 ± 0.005 cm, respectively. Considerable differences in optical and kinetic properties of diabetic and non-diabetic skin were found: clearing efficiency was 1.5-fold better and glucose diffusivity was 2-fold slower for diabetic skin.

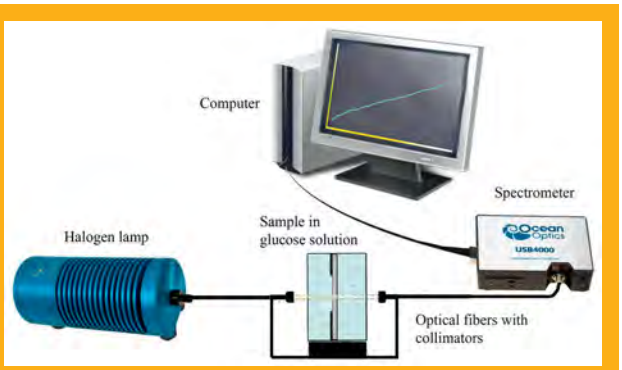

Experimental Setup for measuring collimated transmittance spectra of mouse skin samples.

1. Introduction

Optical methods of monitoring and treatment of tissue properties become more visible and widely applicable in biology and medicine. Their usefulness is due to safety and possibility to obtain a number of parameters in real time and noninvasiveness. Optical methods are extending their scope of application in medicine very rapidly. Functional imaging and monitoring of endogenous (metabolic) and exogenous chemical agents transport in biological tissues are under close attention of investigation during last decade (see for example, monographs and overview papers [1–7]). Permeability of tissues for different agents is studied aiming to get knowledge about mechanisms of tissue interaction with various chemicals, including metabolic molecules, drug transport within tissues, and impact of agents on tissue optical, morphological and functional properties [1–4, 8]. Agent's permeability rate and optical clearing efficiency in a tissue may be indicative for the presence of tissue pathology, such as atherosclerotic vascular disease [3, 9] or cancer [3, 10–14].

* Corresponding author: e-mail: tuchinadk@mail.ru, Phone: +7(8452)210716

Various experimental methods are developed and widely used to study kinetics of tissue optical properties at interaction with the agents [1–4, 8]. A so-called optical clearing (OC) technique can be used for determination of permeability rate of chemical agents in tissues. Optical clearing agents (OCAs) are typically hyperosmotic and have a higher refractive index compared to tissue interstitial fluid (ISF) or cell cytoplasm. Interaction of an OCA with a tissue induces better matching of refractive indices of tissue scattering components (fibers, cell organelles) and their surrounding medium (ISF, cytoplasm) by tissue dehydration and partial replacement of ISF and cytoplasm by the agent. Therefore, OCA application leads to reduction of tissue scattering coefficient and increase of anisotropy factor due to better refractive index matching and packing of tissue components and hence increases probing or acting light penetration depth [1–4]. Optical clearing technique is efficiently used for investigation of different tissues: skin [4, 16–25], skeletal muscle [7, 26, 27], *dura matter* [28], eye sclera [1, 3, 12, 15], stomach [1], breast [11, 13], lung [29] and others [1–3]. Various OCAs were applied for tissue and blood optical clearing such as glucose [1–4, 8, 15, 19, 26, 28], fructose [4], ribose [4], mannitol [28], glycerol [1–4, 8, 16–18], ethylene glycol [27], polyethylene glycol [1, 17] and some others [1–3]. As OCAs and chemical enhancers of their permeability DMSO [18], propylene glycol [17], and thiazone [3, 17] are often used. One of the widely used OCAs is glucose-water solution.

Glucose plays a significant role in the functioning of the living organisms whose primary role is energy delivery. For subsequent regulation of the glucose metabolism, peptide hormone insulin is produced in pancreas by beta cells. If prolonged glucose excess in blood takes place (hyperglycemia), it leads to increase of the glucose level in the ISF of the living body and is associated with *diabetes mellitus* [30–32]. Diabetes is caused by either the pancreas not producing enough insulin (Type 1, insulin-dependent), or the body cells not responding properly to the insulin produced (Type II, non insulin-dependent or "adult-onset diabetes"). Worldwide in 2012 and 2013 diabetes resulted in 1.5 million to 5.1 million deaths per year, making it the 8th leading cause of death [33].

As glucose level in blood is related to its level in the ISF, hyperglycemia contributes to metabolic imbalance and organs disorder [34]. In this connection, many papers are dedicated to determination of free glucose concentration in blood, ISF, and other fluids of the body [2, 35–44], designing of implanted biosensors for continuous monitoring of free glucose [2, 45], study of glucose impact on blood and tissue proteins and designing methods for monitoring of diabetes development based on the differences of optical properties of healthy and diabetic tissues [1, 2, 34, 46–50], quantification of glucose diffusion in healthy [1–3, 8, 26–28, 51] and pathological tissues – atherosclerotic vascular [3, 9] and cancerous tissue [29].

The major complication in diabetics at the advanced stages of the disease is associated with protein glycation. Glycation is a result of glucose molecules interaction with proteins that leads to modification of protein structure and limitation of tissue functioning [46–49]. It is already known that glycation of proteins is initiated by non-enzymatic reaction between amino group of the protein and carbonyl group of the sugar and corresponding protein cross-linking [34, 47, 50]. Advancement of glycation results in Maillard reaction, which includes two stages. In consequence of protein reaction with glucose a stable Amadori product is formed through Schiff base adducts. Upon further incubation, an Amadori product is converted to advanced glycation end product (AGE) [34, 52]. The exact mechanisms of collagen glycation is unclear yet because of complex processes accompanied the reaction [47, 50, 52–54]. But two of AGEs have been already identified: N(ε)-carboxymethyllysine (CML) and pentosidine. CML and pentosine accumulate in the skin collagen with aging and in case of diabetes. Pentosine is a fluorescent molecule and it can be detected by this property [50, 52, 53, 55].

The structural change of a protein molecule influences its optical properties. Since high glucose level in blood results in the elevation of its level in the interstitial fluid, glycation can occur not only with blood proteins such as hemoglobin and albumin, but also with proteins of body tissues. Fluorescence properties of AGEs from hemoglobin, skin, cornea, aorta, articular cartilage have been investigated [47, 49, 53, 55, 56]. It was found that glycation contributes to increasing of tissue fluorescence intensity [47, 53, 55–57] and decreases intensity of the second harmonic generation (SHG) [47, 58]. Vessel wall glycation causes the cross-linking of vessel wall proteins [59]. It was also demonstrated the considerable difference of refractive properties of erythrocytes in diabetic and healthy patients [48]. Intensity of light reflected from the skin of individuals with diabetes depends on the extent of structural differences induced by glycation [60]. It was also shown that *in vivo* NIR spectroscopy of skin is sensitive to tissue glycation and applicable for detection of diabetes mellitus [61, 62].

Proteins are the main components of many tissues, their glycation causes the change of tissue structure significantly [47, 50]. Since tissue permeability for OCAs and metabolic agents is defined by the tissue structure and its alterations due to pathological processes, such as glycation, the measurement of the temporal dependence, for agent diffusion will reflect changes of tissue structure, and thus can be used as a biomarker of degree of tissue glycation. Because all vital organs and tissues, such as myocardium, eye retina, brain tissues, are well supplied with blood,

i.e. with glucose in diabetes, they are exposed to glycation primarily. This is a big challenge to monitor early structural changes of these tissues noninvasively using optical methods. However, because skin is a superficial organ which can be easily investigated optically and skin is also well supplied by blood and contains a big amount of proteins we can propose to use the monitoring of early diabetic changes in human skin to predict the course of the disease development for the whole body, including vital organs.

In this study, optical clearing of skin tissue of healthy mice and mice with *in vivo* alloxan induced diabetes were investigated. Optical clearing was used for determination of glucose diffusion coefficient in diabetic and non-diabetic skin tissue *ex vivo*. The method is based on the measurement of kinetics of optical collimated transmittance of a tissue sample at glucose solution application. The motivation for this study is to quantify diffusion process of glucose in skin *ex vivo* in order to understand its relation to structural change in this tissue due to *diabetes mellitus* development *in vivo*.

2. Materials and methods

2.1 Skin structure and water content

Skin has a complex heterogeneous cell/fiber structure, which defines the high light scattering of the tissue. It includes three layers: epidermis, dermis and subcutaneous fat. The main part of skin is dermis, which mainly consists of collagen fibers (70% of skin dry weight) packed into bundles, elastin and interstitial fluid, which contains proteoglycans, proteins, water and protein-polysaccharide complexes. Skin dermis is well supplied by blood that provides skin absorption in the visible range due to oxy- and deoxyhemoglobin absorption [1]. Diameter of collagen fibers is in the range of 40–150 nm [63]. Two other main visible light absorbers in the skin are melanin and β-carotene, which are contained mostly in epidermis [64].

Tissue water plays an important role for maintenance of structural and mechanical properties of skin and mutual interaction of skin proteins [65], as well as for OCA diffusivity [26, 27]. In the young skin, the majority of water molecules are found in the "bound" form. Water molecules that are not bound to proteins ("protein-bound" water) are bound to each other forming a tetrahedron structure (so-called "bulk" water). Some amount of water in the skin is in a free state that is so-called "free" water. Free water content depends on skin physiological/pathological state, humidity of the environment and skin moisturization by chemical agents [66–68]. Bound water can be transformed into free water at compression and intensive evaporation from the skin surface (dehydration) [69–71]. Confocal Raman microscopy allows for quantification of water distribution along skin depth *in vivo* [72, 73]. In human skin *stratum corneum* water content (mass-%) is 40–45% with gradual increase to 65–70% in deeper layers of living epidermis and dermis. The overall water content in rat skin is found as 54% [74]. However, in literature there is lack of information about quantitative interrelation between protein-bound, bulk and free water for normal and diabetic skin. Absorption properties of skin in the NIR spectral range is determined by absorption of water [1–3, 19]. NIR spectroscopy was used for discrimination of free, bulk, and bound water in skin [75]. Total water content in mouse skin was estimated by NIR spectroscopy as ~70% [76].

2.2 Experimental animals and optical clearing agents

Two month white mice Balb/c with body mass of 20–25 g were used in the study. The investigation was performed on mouse skin samples obtained *ex vivo* by autopsy. To avoid sexual dependence only male mice were used in this investigation. All samples were taken from the back side of animals. Hairs were removed with depilatory cream from each sample before measurements. The hypodermic fatty layer was also removed by tweezers. The area of the samples was about 8 $mm^2 \times 15$ mm^2. The thickness of each sample was measured before and after application of glucose solution in 5 different points by micrometer with a precision of 50 μm and data were averaged.

As optical clearing agents 30%-, 43%-, and 56%-glucose solutions (weight/volume) were used. Aqueous glucose solutions were prepared using glucose monohydrate powder (SCR Co., Ltd., China) and warm distilled water. Refractive indices of solutions (Table 1) were measured at room temperature about 20 °C by Abbe refractometer WAY-2S (Optics Ivy-

Table 1 Refractive indices of glucose solutions.

Glucose concentration	30%	43%	56%
Refractive index at 589 nm	1.379	1.398	1.418
pH	5.2	5.7	6.0

Abbe refractometer accuracy is ± 0.0002

men Systems, Spain). The chosen concentrations are associated with skin water content and used in order to make a possibility to induce different water fluxes at solution application. Therefore, we hypothesized that application of solutions with different concentrations of water may have different impact on skin in dependence on the total amount of water and the balance between free, bulk and bound water in the skin [66, 67, 72–76].

2.3 Protocol for diabetes mellitus animal model

Alloxan-induced diabetes was used as an experimental model of *diabetes mellitus*. Alloxan injection to experimental animals induces the destruction of pancreatic beta islets that causes the abnormality in the insulin production and hence *diabetes mellitus*. The first who described the alloxan-induced diabetes model was Dunn and co-workers in 1943 [77, 78].

In our study *diabetes mellitus* was induced by injection of a single dose of alloxan to experimental animals. To produce alloxan, 1 g of uric acid (TCI Europe N.V., Tokyo, Japan) was added to 2.5 ml of nitric acid (Sinopharm Chemical Reagent Co. Ltd.) step by step; every step required a thorough mixing. Alloxan crystals that are formed in the mixture were filtered, then alloxan crystals were dissolved in warm distilled water at volume fractions of 1 : 1.5 (water temperature was not higher than 60 °C). The warm solution was filtered to the cup and then mixture was dried by hairdryer. The procedure with water addition and drying of mixture was repeated one more time. The obtained alloxan crystals were added to saline in a ratio of 85 mg of alloxan to 2 ml of saline and subcutaneously injected to mice as 212 mg/kg body mass.

The level of glucose in blood taken from the mice tail vein was measured after fasting before alloxan injection on the 4th day after injection and on the day of the experiment (11th day) using glucometer "Accu-Chek Active". The average values of free glucose level in blood before alloxan injection, on the 4th day after injection and on the day of the experiment were 127 ± 18 mg/dL, 276 ± 105 mg/dL and 322 ± 120 mg/dL, respectively.

2.4 Measurement of temporal collimated transmittance spectra of the tissue samples

The measurements of collimated transmittance of tissue samples were performed using commercially available spectrometer USB4000-Vis-NIR (Ocean Optics, USA). The sample was fixed in the cuvette filled up with glucose solution using the plastic plate

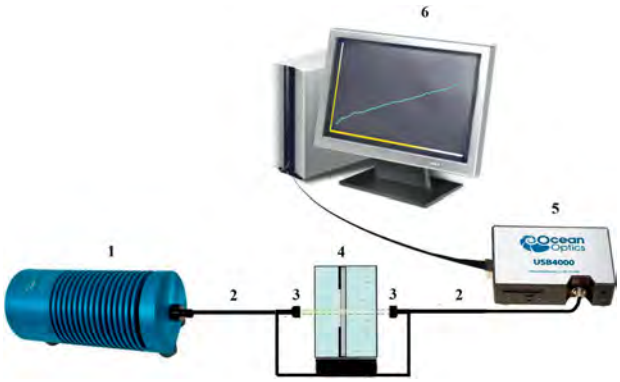

Figure 1 The scheme of the experimental setup for measuring of collimated transmittance spectra of tissue sample immersed in the aqueous glucose solution: halogen lamp HL-2000 (**1**), two optical fibers (**2**) with collimators (**3**), cuvette with the sample placed on the plastic plate that is immersed in solution (**4**), multichannel spectrometer USB4000-Vis-NIR (**5**) and computer (**6**).

with a square aperture of 25 mm^2 in the centre. The cuvette with a sample was placed between two optical fibers with collimators, one of the fibers was used to deliver the radiation to the sample, and another one was used to collect the transmitted light. The spectrometer equipped with optical fibers (QP600-2-VIS-NIR, Ocean Optics, USA) with 600 μm core diameter and collimators 74-UV (Ocean Optics, USA), and the halogen lamp (HL-2000) as a light source were used. The scheme of the experimental setup is presented in Figure 1. The collimated transmittance was recorded every 15–60 sec during 6–10 min in the spectral range of 400–1000 nm. The measurements were performed at room temperature about 20 °C. For each concentration of glucose solution twenty skin samples were tested, ten of them were taken from healthy mice and the other ten – from diabetic mice.

2.5 Quantification of glucose diffusion coefficients

The method of diffusion coefficient estimation is based on the measurement of kinetics of collimated transmittance, which is changed with time due to glucose osmotic action and its diffusion into the tissue [1–4, 8]. Glucose diffusion into the tissue leads to matching refractive indices of tissue scatterers (collagen and elastic fibers) and their environing ISF. In its turn, glucose osmotic action leads to tissue dehydration and therefore to addition contribution in refractive index matching condition and to better packing ability of scatterers [1–3]. Hence kinetics of collimated transmittance is related to rates of glucose diffusion within a tissue sample and induced water flux.

Journal of BIOPHOTONICS

The problem of evaluation of diffusion rate is solved in the framework of the free diffusion model with some hindering due to glucose molecules interaction with tissue structures and involvement of water counter-flow, which are expressed as a mean matter diffusion coefficient. Specially developed software was used to estimate the mean matter diffusion coefficient in skin. The tissue sample model was presented as a plane-parallel slab with a thickness l, cm, which consists of dielectric cylinders (fibrils) providing light scattering. A one-dimensional diffusion equation of a matter transport has the form [1, 2, 79]:

$$\frac{\partial C(x,t)}{\partial t} = D\frac{\partial^2 C(x,t)}{\partial x^2}, \tag{1}$$

where $C(x, t)$ is the glucose concentration in skin sample, g/ml; D is the diffusion coefficient, cm^2/sec; t is the time of diffusion, sec; x is the spatial coordinate along the sample thickness, cm. Surrounding glucose solution amount is much bigger than sample's volume, therefore boundary conditions mean that penetration of glucose into a skin sample does not influence the outside glucose concentration. This requirement has been met in the experiments since the glucose solution volume in the cuvette was about 3000 mm^3 and the volume of the skin samples was less than 150 mm^3. At the study of excised *ex vivo* skin samples during a relatively short time period, glucose diffuses into sample mostly through the dermal side of tissue interface, as the diffusion via epidermal interface could not happened yet during this time because of strong barrier properties of stratum corneum for penetration of the most foreign molecules. Thus, the boundary conditions for one-sided diffusion can be acceptable:

$$C(0,t) = C_0, \qquad \frac{\partial C(l,t)}{\partial x} = 0 \tag{2}$$

where C_0 is the concentration of glucose solution in the cuvette, g/ml, and l is the sample thickness.

The initial conditions correspond to the absence of glucose solution inside the skin sample before its incubation for all inner coordinates of the sample:

$$C(x,0) = 0 \tag{3}$$

The volume-average concentration of glucose in the skin sample $C(x)$ can be derived from Eq. (1) at the boundary (Eq. (2)) and initial (Eq. (3)) conditions as:

$$C(t) = C_0\left(1 - \frac{8}{\pi^2}\sum_{i=0}^{\infty}\frac{1}{(2i+1)^2} \times \exp\left(-(2i+1)^2\, t\, \frac{\pi^2}{4}\, D/l^2\right)\right) \tag{4}$$

In a first-order approximation, the Eq. (4) is reduced to the equation:

$$C(t) \approx C_0(1 - \exp\,(-t/\tau_D)) \tag{5}$$

where

$$\tau_D = \frac{4l^2}{\pi^2 D} \tag{6}$$

is the characteristic diffusion time, sec.

The result of approximation is close to the exact solution (Eq. (4)) in the limits of typical experimental errors, but, at the same time, significantly reduces time of calculation.

The temporal dependence of the refractive index of interstitial fluid $n_I(t)$ can be found from the law of Gladstone and Dale [80], which states that for a non-interacting multi-component system the resulting value of the refractive index represents an average of the refractive indices of the components related to their volume fractions:

$$n_I(\lambda,t) = n_{I0}(\lambda)\cdot(1 - C(t)) + n_G(\lambda)\cdot C(t) \tag{7}$$

where λ is the wavelength, nm; $n_{I0}(\lambda)$ is the wavelength dependence of refractive index of the interstitial fluid at $t = 0$ [81]:

$$n_{I0}(\lambda) = 1.351 + \frac{2134.2}{\lambda^2} + \frac{5.79\times10^8}{\lambda^4} - \frac{8.15\times10^{13}}{\lambda^6} \tag{8}$$

$n_G(\lambda)$ is the wavelength dependence of refractive index of aqueous glucose solution [82]:

$$n_G(\lambda) = n_W(\lambda) + 0.1515\cdot C_0 \tag{9}$$

where $n_W(\lambda)$ is the wavelength dependence of refractive index of water [83]:

$$n_W(\lambda) = 1.3199 + \frac{6.878\times10^3}{\lambda^2} - \frac{1.132\times10^9}{\lambda^4} + \frac{1.11\times10^{14}}{\lambda^6} \tag{10}$$

The scattering coefficient of the skin sample can be estimated as [1, 2, 79, 84]

$$\mu_S(\lambda,t) = \frac{\varphi_S(t)}{\pi a^2}\cdot\sigma_S(\lambda,t)\cdot\frac{(1-\varphi_S(t))^3}{1+\varphi_S(t)} \tag{11}$$

where $\varphi_S(t)$ is the time-dependent volume fraction of scatterers – a monodisperse ensemble of long dielectric cylinders modeling collagen and elastin fi-

bers; a is their radius; $\sigma_S(\lambda,t)$ is the time-dependent scattering cross-section [85]:

$$\sigma_S(\lambda,t) = \frac{\pi^2 a \cdot x^3(\lambda,t)}{8}\,(m^2(\lambda,t)-1)^2 \times \left(1+\frac{2}{(m^2(\lambda,t)+1)^2}\right) \quad (12)$$

where $m(\lambda,t) = n_S(\lambda)/n_I(\lambda,t)$ is the ratio of the refractive indices of the collagen/elastin fibers ($n_S(\lambda)$) and surrounding medium ($n_I(\lambda,t)$), and $x(\lambda,t) = 2\pi a n_I(\lambda,t)/\lambda$ is the size parameter.

The wavelength dependence of refractive index of the collagen/elastin fibers is determined as [28]:

$$n_S(\lambda) = 1.439 + \frac{15880.4}{\lambda^2} - \frac{1.48\times 10^9}{\lambda^4} + \frac{4.39\times 10^{13}}{\lambda^6} \quad (13)$$

The initial volume fraction of the scatterers φ_{S0} was obtained from initial mass and initial volume of the investigated samples:

$$\begin{cases} W_s + W_{\mathrm{ICF}} = W_0 \\ V_s + V_{\mathrm{ICF}} = V_0 \end{cases} = \begin{cases} V_s\rho_s + V_{\mathrm{ICF}}\rho_{\mathrm{ICF}} = W_0 \\ V_s + V_{\mathrm{ICF}} = V_0 \end{cases} \quad (14)$$

where W_s is the mass of skin scatterers, W_{ICF} is the mass of skin interstitial fluid, V_s is the volume occupied by the skin scatterers, W_{ICF} is the volume occupied by the skin interstitial fluid, W_0 and V_0 are the mass and the volume of the sample measured at $t=0$ (see Section 2.6), $\rho_s = 1.41$ [86] and $\rho_{\mathrm{ICF}} \approx 1$ [87] is the mass density of the skin scatterers and the skin interstitial fluid. From Eq. (14) we can find that $V_s = V_0 - \dfrac{V_0\rho_s - W_0}{\rho_s - \rho_{\mathrm{ICF}}}$ and $\varphi_{S0} = V_s/V_0$.

The experimental temporal dependences of the sample thickness $l(t)$ and area $S(t)$ were used to account changes of the skin sample volume $V(t)$ and the volume fraction of the scatterers $\varphi_S(t)$: $\varphi_S(t) = \varphi_{S0}V_0/V(t)$, where $V_0 = S_0 \cdot l_0$, and $V(t) = S(t)\cdot l(t)$.

The mean diameter of skin fibers $2a$ was estimated from Eq. (11) for different samples as 120–130 nm by substituting the initial value of the scattering coefficient, which was obtained from the equation:

$$\mu_{S0} = -\frac{\ln\,(T(t=0))}{l_0} - \mu_{a0} \quad (15)$$

where μ_{a0} and μ_{S0} are the initial absorption and scattering coefficients, respectively, l_0 is the initial thickness of the sample. The obtained data for the tissue fiber mean diameter fit well the human skin fiber diameter measured directly using electronic microscopy for normal skin as 40–150 nm [63]. In this study, we assume that initial absorption coefficient is equal to that of rat skin [88].

The temporal dependence of the absorption coefficient $\mu_a(t)$ was obtained from the equation:

$$\mu_a(t) = \varphi_S(t)\cdot\sigma_{a0}/\pi a^2 \quad (16)$$

where σ_{a0} is the absorption cross section, which can be determined from the initial values of μ_{a0} and φ_{S0} for each wavelength.

The time-dependent collimated transmittance of the sample at optical clearing is defined as:

$$T_c(t) = \exp\left[-(\mu_a(t)+\mu_S(t))l(t)\right] \quad (17)$$

By using measurement of temporal collimated transmittance of mouse skin samples, the inverse problem solution has been obtained as the reconstruction of the diffusion coefficient of glucose in skin by minimization of the following target function:

$$f(D) = \sum_{i=1}^{N_t} (T_c(D,t_i) - T_c^*(t_i))^2 \quad (18)$$

where $T_c(D, t_i)$ and $T_c^*(t_i)$ are the calculated and experimental values of the time-dependent collimated transmittance; N_t is the sampling number at registration of the temporal dependence of collimated transmittance.

We have to note that Eq. (17) assumes both absorption and scattering coefficients to be spatially uniform for a given time moment. The assumption is valid because in the course of measurements, attenuation coefficient is automatically averaged along collimated light beam that is tracing the sample. Thus, the measured kinetics describes behavior of the spatially averaged attenuation coefficient with dominating inclusion of the scattering coefficient ($\mu_a \ll \mu_s$).

For minimization of the target function, the Levenberg–Marquardt nonlinear least-squares-fitting algorithm described in detail by Press et al. [89] has been used. Iteration procedure was repeated until experimental and calculated data were matched with a desirable precision. As a termination condition of the iteration process, we have used the following expression:

$$\frac{1}{N_t}\sum_{i=1}^{N_t}\frac{|T_c(D,t_i) - T_c^*(t_i)|}{T_c^*(t_i)} \le 0.01 \quad (19)$$

2.6 Quantification of skin sample dehydration ability

For quantification of dehydration ability of skin samples under study during optical clearing, the thickness of non-diabetic skin samples was measured using a confocal microscope (FV 1000, Olympus, Japan) at application of glucose solutions. The tissue sample was placed on the glass substrate by the epidermis side and the thickness of intact sample was measured. After that, glucose solution was dripped on the sample to cover it. Sample thickness was measured every 20–50 sec during 15–20 min. The measurements were performed for 30 skin samples of healthy mice under action of 30%-, 43%- and 56%-glucose solution, 10 samples for each solution.

The mass of intact skin samples was also measured during action of glucose solutions using weight scale (PL203, Mettler Toledo, China) with the precision of 1 mg. The area of each sample was measured concurrently by processing of obtained successive digital images (Figure 2a) of the sample. Correspondingly, 30 samples were measured at immersion in 30%-, 43%- and 56%-glucose solutions, 10 samples for each solution. The measurements of the sample mass and digital images were made every 5 min during 15 min of immersion.

The temporal dependences of tissue dehydration were obtained from the data on mass, thickness and area of a sample under optical clearing. To estimate the sample area the color hue component of digital image was obtained by the READ_HLS_HUE function of MathCad software (Parametric Technology Corporation, USA). The example of the calculation was presented in Figure 2b. The median filter was used to reduce the noise, glare and differential brightness (Figure 2c). The range of the hue-component was selected to make the area around the sample white colored (Figure 2d). The processed image was used to calculate the number of pixels occupied by the sample and to convert them into the square millimeters:

$$S = \frac{F(H_s)}{\mathrm{cols}(H_S)\cdot \mathrm{rows}(H_S)} \cdot \frac{\mathrm{rows}(H)\cdot z^2}{\mathrm{cols}(H)} \qquad (20)$$

where function F counts the pixels occupied by the sample, cols is the number of columns, rows is the number of rows, H_S is the processed image of the sample with a white background, H is the original image, z is the width of the image.

3. Experimental results

To estimate the glucose diffusion coefficients in both diabetic and non-diabetic skin the temporal dependencies of the collimated transmittance of *ex vivo* skin samples immersed in glucose solutions of different concentration were measured. The typical collimated transmittance spectra of three non-diabetic and three diabetic skin samples immersed in 30%-, 43%-, and 56%- glucose solutions are presented in Figure 3, respectively left and right panels. Typical graphs for six samples illustrating temporal behavior of these spectra at glucose concentration variation are presented. Results on quantification and averaging accounting for difference in thickness for 60 samples are summarized in Tables 2 and 3. It can be seen that untreated samples poorly transmit light. For all skin samples, both non-diabetic and diabetic, collimated transmittance is increasing with the wavelength in the studied spectral range from 450 nm to 950 nm. Skin samples were rather bloodless, thus no hemoglobin absorption bands are seen, mostly light scattering influence the spectral shape of the transmittance. The measured spectra were used to obtain temporal dependencies of collimated transmittance of the skin samples at a particular wavelength and their further processing to get optical clearing efficiency, diffusion and permeability coefficients.

The typical temporal dependencies of collimated transmittance for six skin samples immersed in glucose solutions measured at different wavelengths are presented in Figure 4. For both types of skin samples from normal and diabetic mice, the collimated transmittance increases with time (optical clearing process), i.e. attenuation of the light beam decreases. This is mostly caused by tissue dehydration, induced by osmotic properties of glucose, and matching of refractive indices of collagen fibers and due to glucose diffusion into the ISF [4, 16–25, 90]. For longer

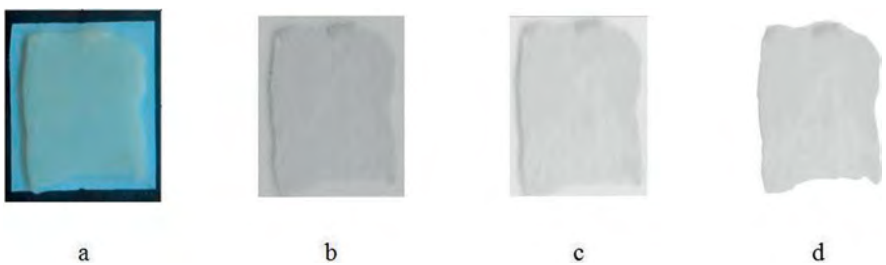

Figure 2 The digital image of skin sample (**a**), the color hue-component image (**b**), the image processed by median filter (**c**), processed image of the sample with a white background (**d**).

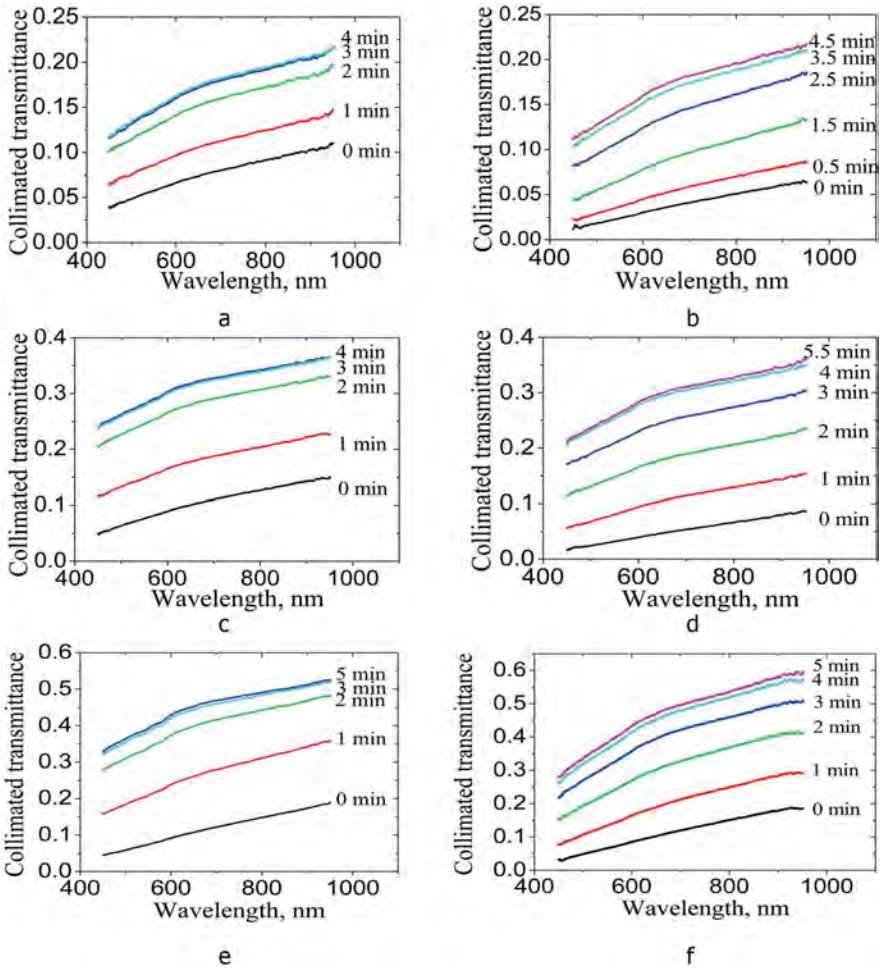

Figure 3 Collimated transmittance spectra of non-diabetic (**a**, **c**, **e**) and diabetic (**b**, **d**, **f**) skin samples during treatment by 30%- (**a**, **b**), 43%- (**c**, **d**), and 56%- (**e**, **f**) aqueous glucose solutions measured in different time intervals.

time, the elevation of collimated transmittance is saturated, indicating the saturation of diffusion processes in the system and establishment of some equilibrium state between induced fluxes (mostly glucose and water).

Such temporal behavior of optical properties with saturation, in the limits of differences of the used animal model and optical clearing agents, corresponds well with the earlier published data [90], where interrelations between clearing ability (drop of reduced scattering coefficient), dehydration and thickness of porcine skin samples were studied for several hyperosmotic optical clearing agents. Being in general similar to results of previous studies, the data pre-

Table 2 The efficiency of optical clearing of healthy and diabetic mouse skin expressed as relative change of averaged transmittance for all studied skin samples and all wavelengths (second column) and as estimated relative change of the averaged scattering coefficient (third column), T_{max} is the maximal averaged transmittance, T_0 is the initial averaged transmittance, μ_{s0} is the initial averaged scattering coefficient, and μ_{smin} is its minimal value.

Glucose solution	$\frac{T_{max} - T_0}{T_0}$	$\frac{\mu_{s0} - \mu_{s\,min}}{\mu_{s0}}$
Non-diabetic skin		
30%	2.26 ± 0.65	0.34 ± 0.07
43%	2.84 ± 1.58	0.52 ± 0.09
56%	6.91 ± 2.95	0.62 ± 0.04
Diabetic skin		
30%	4.82 ± 1.86	0.42 ± 0.06
43%	4.46 ± 1.73	0.51 ± 0.05
56%	9.07 ± 3.80	0.53 ± 0.12

± – standard deviation

Table 3 Kinetic parameters for dehydration and shrinkage of healthy mouse skin samples.

Glucose solution	Number of samples	Mass/Dehydration		Thickness/'transverse shrinkage'		Area/'along shrinkage'	
		H (∞)	τ_D^w, min	A_D^l	τ_D^l, min	A_D^S	τ_D^S, min
30%	10	0.23 ± 0.01	4.51 ± 0.61	0.27 ± 0.01	2.75 ± 0.21	0.07 ± 0.04	12.20 ± 12.00
43%	10	0.16 ± 0.01	5.86 ± 1.10	0.16 ± 0.01	3.10 ± 0.42	0.17 ± 0.01	6.80 ± 1.40
56%	10	0.27 ± 0.02	2.91 ± 0.87	0.37 ± 0.01	4.28 ± 0.40	0.09 ± 0.01	7.20 ± 0.20

± – standard deviation

sented in Figure 4 and Table 2 give new important information about considerable differences in optical clearing efficiency and kinetics of diabetic and non-diabetic skin. The optical clearing of diabetic skin takes some more time for saturation (5–6 min) compared to non-diabetic skin (about 3 min).

The degree (efficiency) of optical clearing of healthy and diabetic skin samples was evaluated as the ratio of the difference between the maximal (within the saturation region of the kinetic curve, Figure 4) and the initial transmittance to the initial transmittance. It was also evaluated as the ratio of the difference between the minimally achieved and the initial scattering coefficient values to the initial scattering coefficient value, all obtained from transmittance data by Beer–Lambert–Bouguer law. These data were averaged by wavelength and by the samples (Table 2). The considerable difference in optical and kinetic properties of diabetic and non-diabetic skin is well seen. It follows from Table 2 that the optical clearing efficiency is less for healthy skin than for diabetic skin. Diabetic skin is more responsive to

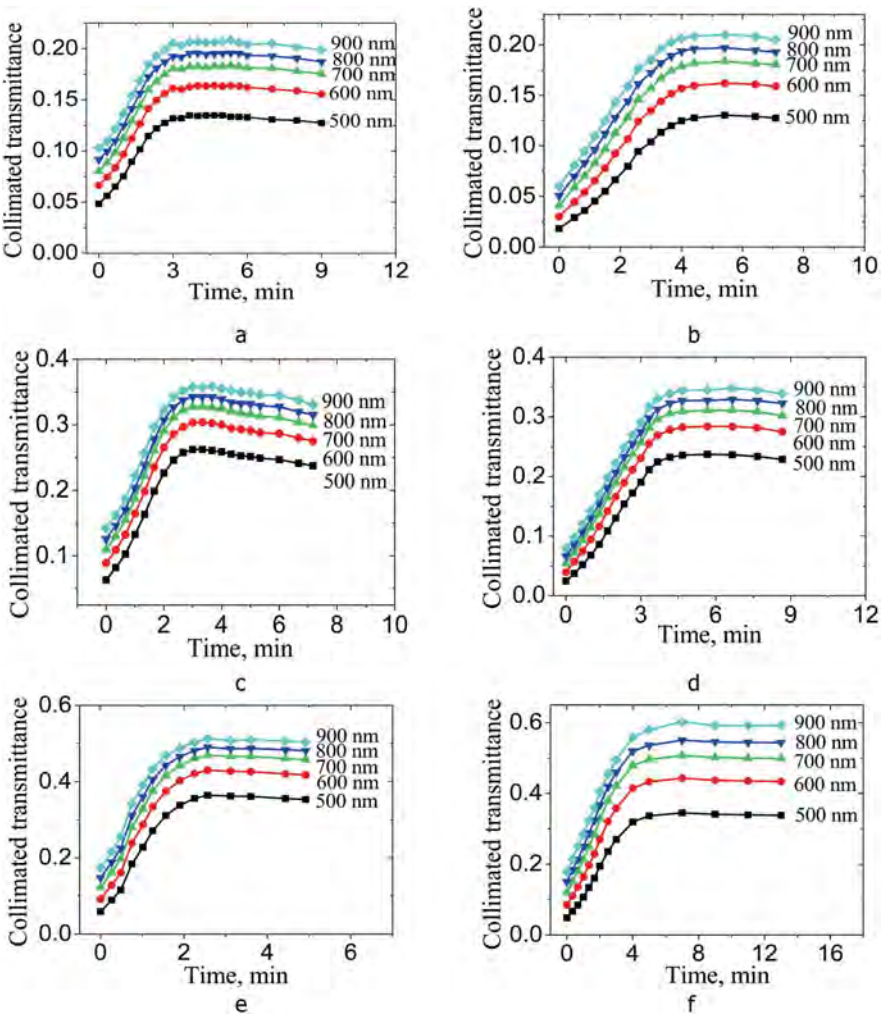

Figure 4 Collimated transmittance kinetics of non-diabetic (**a**, **c**, **e**) and diabetic (**b**, **d**, **f**) skin samples during treatment by 30%- (**a**, **b**), 43%- (**c**, **d**), and 56%- (**e**, **f**) aqueous glucose solutions measured for different wavelengths.

glucose uploading with up to 2-fold bigger clearing efficiency against normal skin.

In general, higher glucose concentration leads to better optical clearing for both types of skin (see Table 2), yet having some specific features related to different response of sample thickness of normal and diabetic tissues to glucose dehydration ability. All these discoveries could be associated with structural changes in the skin dermis proteins and balance between free and bound water for diabetic skin related to normal skin.

To evaluate diffusion coefficient precisely, tissue sample thickness should be measured in the course of optical clearing because of tissue time-dependent shrinkage. Information about tissue shrinkage and corresponding mass change are also important to propose mechanisms of optical clearing and glucose diffusivity in healthy and diabetic tissues. The temporal dependences of normalized change of thickness and area of skin samples $A(t)$ during action of glucose solutions can be approximated by the following equation which is similar to Eq. (5), because tissue shrinkage behavior is related to diffusion processes in tissues

$$A(t) = \frac{A(t=0) - A(t)}{A(t=0)} = A_D(1 - \exp(-t/\tau_D)) \quad (21)$$

where A_D is the final thickness or area of the skin sample and τ_D is characteristic diffusion time; A_D^l and τ_D^l are parameters for sample thickness l, as A_D^S and τ_D^S – for area S. Tissue shrinkage can be characterized by 'along shrinkage' and 'transverse shrinkage', i.e., along or transverse to dermal fibers which are lying along skin surface. 'Along shrinkage' is estimated from area measurements and 'transverse shrinkage' – from measurements of thickness (see Figure 5, Table 3).

Kinetics of skin sample dehydration was calculated from the sample mass measured in the course of its impregnation by glucose (Figure 5, Table 3). Degree of tissue sample dehydration $H(t)$ was defined as:

$$H(t) = \frac{W(t=0) - W(t)}{W(t=0)} = H(\infty)(1 - \exp(-t/\tau_D^w)) \quad (22)$$

where $W(t = 0)$ and $W(t)$ are the mass at the initial time and current time t after skin sample immersion in glucose solution, respectively; $H(\infty)$ is the constant, which characterizes the maximal degree of dehydration, and τ_D^w is the characteristic dehydration time. Similar form of equation as Eqs. (21) or Eqs. (22) is also applicable to approximate kinetics of optical transmittance.

It is seen from Figure 5 and Table 3 that normalized variation of mass, thickness and area of skin samples increases (absolute values of mass, thickness and area decrease) at glucose action. Changes of the sample properties at application of 30%- and 56%-glucose solutions are more or less similar, as 43%-glucose solution provides some specificity at its action on the sample by inducing the lesser decrease of tissue thickness (lesser 'transverse shrinkage') and mass (lesser dehydration), but bigger decrease of the sample area (bigger 'along shrinkage'). The obtained temporal dependences were used for estimation of diffusion coefficients by taking into account the variations of tissue geometry and mass in the course of optical clearing.

Table 4 summarizes experimental data for both diabetic and non-diabetic skin specimens, including measurements of thickness l; estimates of glucose diffusion coefficients D and D_1 using described above comprehensive algorithm (Eqs. (4) and (7)–(19))

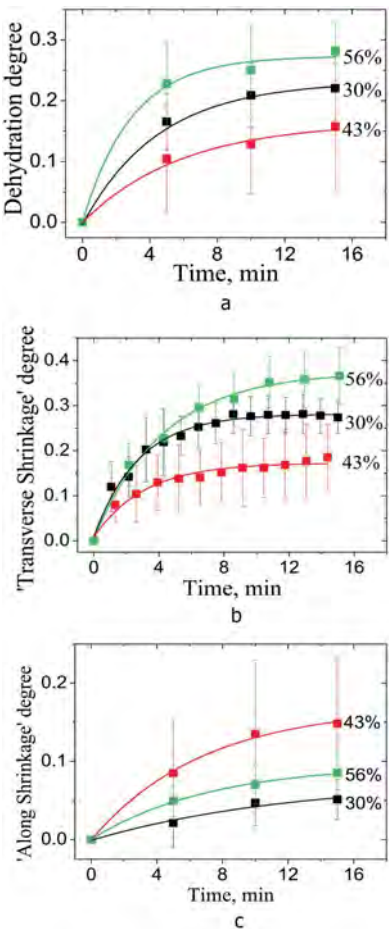

Figure 5 The temporal dependencies of the dehydration degree obtained from the mass kinetics (**a**), the 'transverse shrinkage' degree obtained from the thickness kinetics (**b**), the 'along shrinkage' degree obtained from the area kinetics (**c**) of healthy skin samples under action of 30%-, 43%- and 56%-glucose solutions.

Table 4 Glucose diffusion coefficients in mouse skin: D is estimated from experimental data using a comprehensive algorithm (Eqs. (4) and (7)–(19)), D_1 – using a simple algorithm (Eqs. (6) and (21)); corresponding permeability coefficients $P = D/l_{aver}$ and $P_1 = D_1/l_{aver}$, τ is the measured diffusion time, l is the measured specimen thickness before and after immersion in glucose solution, and K_{max} is the maximal specimen transmittance.

Glucose solution	D (cm²/sec)/ P (cm/sec)	D_1 (cm²/sec)/ P_1 (cm/sec)	τ (min)	l (cm) (before/after)	$K_{max} = T_{max} - T_0$
Non-diabetic mice					
30%	$(2.87 \pm 1.53) \times 10^{-6}$/ $(1.15 \pm 0.61) \times 10^{-4}$	$(2.60 \pm 1.15) \times 10^{-6}$/ $(1.04 \pm 0.46) \times 10^{-4}$	1.99 ± 1.36	$0.027 \pm 0.005/0.023 \pm 0.005$	0.130 ± 0.047
43%	$(2.70 \pm 2.22) \times 10^{-6}$/ $(1.29 \pm 1.06) \times 10^{-4}$	$(2.36 \pm 1.85) \times 10^{-6}$/ $(1.12 \pm 0.88) \times 10^{-4}$	1.88 ± 0.96	$0.023 \pm 0.005/0.019 \pm 0.005$	0.336 ± 0.109
56%	$(1.40 \pm 0.96) \times 10^{-6}$/ $(8.24 \pm 5.64) \times 10^{-5}$	$(1.26 \pm 0.86) \times 10^{-6}$/ $(7.41 \pm 5.06) \times 10^{-5}$	2.15 ± 0.88	$0.019 \pm 0.005/0.015 \pm 0.005$	0.334 ± 0.044
Diabetic mice					
30%	$(1.06 \pm 0.55) \times 10^{-6}$/ $(5.43 \pm 2.82) \times 10^{-5}$	$(1.03 \pm 0.44) \times 10^{-6}$/ $(5.28 \pm 2.26) \times 10^{-5}$	2.87 ± 0.68	$0.021 \pm 0.005/0.018 \pm 0.005$	0.160 ± 0.033
43%	$(1.15 \pm 0.63) \times 10^{-6}$/ $(5.90 \pm 3.23) \times 10^{-5}$	$(9.10 \pm 5.14) \times 10^{-7}$/ $(4.67 \pm 2.64) \times 10^{-5}$	2.98 ± 1.88	$0.020 \pm 0.005/0.019 \pm 0.005$	0.210 ± 0.032
56%	$(1.02 \pm 0.44) \times 10^{-6}$/ $(6.58 \pm 2.84) \times 10^{-5}$	$(8.83 \pm 4.42) \times 10^{-7}$/ $(5.70 \pm 2.85) \times 10^{-5}$	2.80 ± 1.54	$0.017 \pm 0.005/0.014 \pm 0.005$	0.258 ± 0.092

± – standard deviation

and simple one (Eqs. (6) and (21)), respectively; corresponding permeability coefficients $P = D/l_{aver}$ and $P_1 = D_1/l_{aver}$ (where l_{aver} is the averaged thickness) [91]; diffusion time τ obtained from the kinetic curves for collimated transmittance; and maximal specimen transmittance $K_{max} = T_{max} - T_0$.

Glucose diffusion coefficient in diabetic skin is less than in healthy skin for each of tested glucose concentrations. We have to note that a comprehensive algorithm (Eqs. (4) and (7)–(19)) and more simple one (Eqs. (6) and (21)) give very similar results and both allow us to prove the hypothesis that at diabetes glucose diffuses in skin much more slowly, up to 2.5-fold, than in native tissue. As the diffusion coefficients obtained by two methods have a good correlation between them, thus a simple processing technique could be in use for some practical cases, where fast estimations of diffusion or permeability coefficients are needed.

The diffusion coefficient decreases with glucose solution strengthening for non-diabetic skin. That can be connected with the specific free/bulk/bound water content in healthy tissue. Approximately twice lower diffusivity at glucose concentration of 56%-regarding to 30%- and 43%-glucose could mean that an equilibrium of water fluxes [26, 27] from skin out and from solution inside skin is established at this concentration. If we accept that healthy skin contains 54% of water [74] and suppose that there is 10% of protein bound water in skin, an equilibrium in water fluxes can be achieved exactly by application of 56%-glucose solution, since its water concentration is approximately equal to free water content in the skin tissue.

From the other hand, for diabetic skin we see with evidence a weak dependence of glucose diffusion coefficient on concentration that could be due to bigger amount of free/bulk water in pathological skin and its stronger capability to transform from bound/bulk to free form of water in response to osmotic pressure of applied glucose solutions [69, 70].

We also see that thickness of skin samples is reduced after immersion in glucose solutions, average thickness of healthy and diabetic skin reduced from 0.023 ± 0.006 cm to 0.019 ± 0.005 cm and from 0.019 ± 0.005 cm to 0.015 ± 0.005 cm, respectively. It can be seen that both healthy and diabetic skin are equally sensitive to shrinkage (dehydration).

4. Discussion

In our measurements, the lower initial collimated transmittance was found systematically for diabetic skin rather than for normal skin with a similar thickness. This corresponds to the results of Kim et al. [58], where the increase of scattering and diffuse reflectance of glycated human tendon was detected. Therefore, we also prove that diabetic tissue (skin) is a more scattering tissue compared to non-diabetic. The difference of light reflectance for normal and diabetic skin caused by protein glycation was also discussed in review paper by Khalil [60].

The measured spectra (see Figure 3) demonstrate less light transmittance for the shorter wavelength range that is due to higher tissue scattering and absorption of blood residuals in the region from 500 nm to 600 nm and drop of scattering and absorption with the wavelength increase [92].

The greater optical clearing efficiency obtained for the diabetic skin can be explained by a lesser initial transparency of glycated (diabetic) tissue. The change of skin optical properties was caused by its structural modification occurred under pathological conditions. It was shown that glycation leads to loss in axial fibril packing of type I collagen because of twisting and distorting the matrix by adducts of glycation [55, 58, 93, 94].

The greater amounts of skin water content were detected for diabetics compared to non-diabetic subjects [95]. Growth of water in diabetic skin could also be the reason of higher light scattering. Slower glucose diffusion in diabetic skin obtained in our study should be connected with modification of tissue structure in diabetic conditions – loss of fibril packing, growth of protein cross-linking and changes of free and bound water content in skin. The solution strengthening (glucose concentration increase) causes the growth of optical clearing efficiency and reduction of glucose diffusion coefficient. Therefore, the application of more concentrated glucose solutions allows one to reach a stronger optical clearing effect. However, maximal optical clearing is obtainable for longer time due to slower diffusion processes caused by additional impact of concentrated glucose on tissue in the course of diffusion.

As skin tissue contains a large amount of water, the measured glucose diffusion coefficient in skin is interesting to compare with glucose diffusion coefficient in water. For a low concentrated glucose diffusion in water $D_{\text{glucose/water}} = 6.7 \times 10^{-6}$ cm^2/sec at 25 °C [96]. It is a few times bigger than glucose diffusion coefficient measured in skin (Table 4). Slowing down of glucose diffusion in skin is the result of glucose interaction with tissue components (matrix) which is bigger for diabetic skin.

The dependence of skin diffusion coefficient on glucose concentration indicates the involvement of water flux, which should be different for different solutions. The diffusion time τ increase in accordance with growth of solution concentration can be related to mean total water content in skin (~54–60%) [72–74, 97]. The specific balance of free and bound water in the skin should also play a definite role. The amount of free and bulk water in skin can be estimated as 38–44% [72–74, 97], which is approximately comparable with water content of 56%-glucose solution. In this particular case of water balance in tissue and in applied solution, water does not displace much, the diffusion is slow and can be related to glucose molecules only, since water molecules diffuse faster than glucose and their inclusion in diffusion should be small. If skin water content increases in diabetes, the amount of free water could come bigger and more or less equal to water content for 43%-glucose that shows the biggest diffusion time τ at glycation (see Table 4).

The nonlinear behavior of optical clearing efficiency and diffusion time (see Tables 2 and 4) with glucose concentration can be explained by a specificity of skin tissue response to application of glucose solutions of the particular concentration in relation to skin water content. Recently, Luis et al. [26] showed a strong nonlinear dependence of diffusion time in muscle tissue on glucose concentration.

The partial contribution in the nonlinearity of these parameters is made by tissue 'along' and 'transverse' shrinkage. Different shrinkage abilities were obtained for applied solutions and skin conditions (see Table 3). The effect can be also partly associated with pH level of glucose solutions (see Table 1).

Because of lack of information about water status in many tissues and due to importance of the problem, different approaches should be welcome to solve it experimentally. Tissue refractive index measurements using OCT technique [97] at action on a tissue of hyperosmotic agents, heating (tissue drying) and mechanical compression may help to quantify free, bulk and protein-bound water. Multiphoton and CARS imaging may also help in evaluation of protein-bound water content in the course of OCA or mechanical compression action and its transform into bulk and free water [98–100].

In comparison with glucose diffusion coefficient in muscle tissue, which is $(8.83 \pm 4.42) \times 10^{-7}$ cm^2/sec for 40%-glucose solution [26], the values obtained in this study are approximately twice higher. This can be caused by less water content in skin and its multilayer structure with water concentration gradient across the skin layers, as well as by specificity of muscle cell structure. However, the general behavior of tissue kinetics is similar.

In vitro investigations of glycation of tissue and blood proteins by incubation in solutions of ribose [47, 101], or glucose [102, 103] are showing rather efficient glycation of proteins during 10–11 days of incubation. Studies of human placental collagen IV [101], bovine skin collagen [47], and hemoglobin [102, 103] are available in literature. Since alloxan induces hyperglycemia in about 1–3 days after injection [104], we found a well-detectable increase of free glucose in blood on the 4$^{\text{th}}$ day after injection. We supposed that 11 days of hyperglycemia duration may cause partial tissue disorders, and we actually obtained alterations of tissue properties in the diabetic group compared to the control group. For this time-period, in the used animal model we have realized at least the prediabetic conditions. From the diagnostical point of view, it could be especially valu-

able, because optically we can detect initial changes in skin tissues associated with diabetes development on the earlier stage.

Unfortunately, on the early stage of pathology development, the stationary skin optical properties are not so sensitive to glycation. Indeed, we see some difference in initial transmittance between normal and glycated skin (see Figure 4). However, the proposed technique of kinetic measurement of skin optical transmission at glucose diffusion is much more sensitive to alterations of tissue structural properties and is more informative as, in addition to difference in optical clearing efficiency; it gives information about characteristic time of agent diffusion.

5. Conclusion

The presented results show that application of glucose solutions is useful for controlling optical properties of such tissue as skin. The significant difference between optical and kinetic properties of non-diabetic and diabetic skin was observed. It was discovered that the optical clearing of diabetic skin is more effective than non-diabetic, but it is achieved for longer time. Thereby the estimated glucose diffusion coefficients are less for diabetic skin. The diffusion coefficient decreases with the increase of solution concentration for non-diabetic skin and is less dependent on concentration for diabetic.

This work, along with papers [26, 27, 96], has proved that kinetics of exogenous agent diffusion in different tissues is related to involvement in the diffusion process of tissue water and dependent on the balance between free, bulk and protein-bound water in a particular tissue.

Further work needs to be carried out for *in vivo* skin optical clearing. Once the similar difference in non-diabetic and diabetic skin *in vivo* is proved, it will be helpful for evaluation of pathophysiologic state of diabetic. In addition, the blood flow visibility due to *in vivo* skin optical clearing will not only show higher resolution for microvessel structure, but also provide the skin blood flow dynamic parameters by combining with laser speckle contrast imaging [105, 106], which will be a very useful technology especially for investigation of diabetes.

The obtained results may be used for improvement of biophysical and mathematical models describing interactions between normal/diabetic tissues and chemical agents, for optimization of tissue optical clearing and drug delivery techniques, and thus for monitoring of diabetes development and treatment in humans.

Acknowledgements This work was partly supported by Britton Chance Center for Biomedical Photonics of Huazhong University of Science and Technology, Wuhan, China, NSFC-RFBR for International Cooperation (Grant No. 812111313), the Science Fund for Creative Research Group (Grant No. 61121004), grants of Russian Foundation for Basic Research (13-02-91176-ГФЕН_а), Russian Presidential grant NSh-703.2014.2, and The Tomsk State University Academic D.I. Mendeleev Fund Program.

The authors thank Dr. S.V. Eremina (Department of English and Intercultural Communication of Saratov State University) for the help in manuscript translation to English, and Prof. O. V. Semyachkina-Glushkovskaya for her suggestion to use Alloxan diabetes animal model and other advises.

Author biographies Please see Supporting Information online.

References

[1] V. V. Tuchin, Optical Clearing of Tissues and Blood, PM 154 (SPIE Press, Bellingham, WA, 2006).
[2] V. V. Tuchin (ed.), Handbook of Optical Sensing of Glucose in Biological Fluids and Tissues (Taylor & Francis Group LLC, CRC Press, 2009).
[3] D. Zhu, K. V. Larin, Q. Luo, and V. V. Tuchin, Laser Photonics Rev. **7**(5), 732–757 (2013).
[4] J. Wang, N. Ma, R. Shi, Y. Zhang, T. Yu, and D. Zhu, IEEE J. Select. Tops Quant. Electr. **20**(2), 7101007-1–7 (2014).
[5] E. A. Genina, A. N. Bashkatov, and V. V. Tuchin, Expert Rev. Med. Devices **7**(6), 825–842 (2010).
[6] E. A. Genina, A. N. Bashkatov, K. V. Larin, and V. V. Tuchin, in: F. S. Pavone (ed.), Laser Imaging and Manipulation in Cell Biology (Wiley-VCH Verlag GmbH & Co. KGaA, Weinheim, 2010) pp. 115–164.
[7] O. Nadiarnykh and P. J. Campagnola, in: F. S. Pavone and P. J. Campagnola (eds.), Second Harmonic Generation Imaging: SHG and optical clearing (CRC Press, Taylor & Francis Group, Boca Raton, London, NY, 2014), pp. 169–189.
[8] M. G. Ghosn, N. Sudheendran, M. Wendt, A. Glasser, V. V. Tuchin, and K. V. Larin, J. Biophoton. **3**(1–2), 25–33 (2010).
[9] M. G. Ghosn, E. F. Carbajal, N. A. Befrui, and K. V. Larin, J. Biomed. Opt. **13**, 010505 (2008).
[10] E. Galanzha, M. Kokoska, E. Shashkov, J. Kim, V. Tuchin, and V. Zharov, J. Biophoton. **2**, 528–539 (2009).
[11] H. Q. Zhong, Z. Y. Guo, H. J. Wei, C. C. Zeng, H. L. Xiong, Y. H. He, and S. H. Liu, Laser Phys. Lett. **7**, 315–320 (2010).
[12] Q. L. Zhao, J. L. Si, Z. Y. Guo, H. J. Wei, H. Q. Yang, G. Y. Wu, S. S. Xie, X. Y. Li, X. Guo, H. Q. Zhong, and L. Q. Li, Laser Phys. Lett. **8**(1), 71–77 (2011).
[13] Z. Zhu, G. Wu, H. Wei, H. Yang, Y. He, S. Xie, Q. Zhao, and X. Guo, J. Biophoton. **5**, 1–8 (2012).
[14] H. J. Wei, G. Wu, Z. Guo, H. Yang, Y. He, S. Xie, and X. Guo, J. Biomed. Opt. **17**(11), 116006 (2012).

[15] E. A. Genina, A. N. Bashkatov, Yu. P. Sinichkin, V. V. Tuchin, Quant. Electr. **36**(12), 1119–1124 (2006).
[16] E. A. Genina, A. N. Bashkatov, A. A. Korobko, E. A. Zubkova, V. V. Tuchin, I. Yaroslavsky, and G. B. Altshuler, J. Biomed. Opt. **13**(2), 021102-1–8 (2008).
[17] Z. Zhi, Z. Han, Q. Luo, and D. Zhu, J. Innov. Opt. Health Sci. **2**(3), 269–278 (2009).
[18] R. Samatham, K. G. Phillips, and S. L. Jacques, J. Innov. Opt. Health Sci. **3**, 183–188 (2010).
[19] E. A. Genina, A. N. Bashkatov, and V. V. Tuchin, in: V. V. Tuchin (ed.), Handbook of Optical Sensing of Glucose in Biological Fluids and Tissues (Taylor & Francis Group LLC, CRC Press, 2009), pp. 657–692.
[20] A. M. Fox, D. G. Diven, K. Sra, A. Boretsky, T. Poonawalla, A. Readinger, M. Motamedi, and R. J. McNichols, Lasers Surg. Med. **41**, 251–255 (2009).
[21] A. K. Bui, R. A. McClure, J. Chang, C. Stoianovici, J. Hirshburg, A. T. Yeh, and B. Choi, Lasers Surg. Med. **41**(2), 142–148 (2009).
[22] X. Guo, Z. Guo, H. Wei, H. Yang, Y. He, S. Xie, G. Wu, H. Zhong, L. Li, and Q. Zhao, Laser Phys. **20**(9), 1849–1855 (2010).
[23] H. Zhong, Z. Guo, H. Wei, C. Zeng, H. Xiong, Y. He, and S. Liu, J. Biomed. Opt. **15**(3), 036012 (2010).
[24] J. Yoon, D. Park, T. Son, J. Seo, J. S. Nelson, and B. Jung, Lasers Surg. Med. **42**(5), 412–417 (2010).
[25] X. Wen, Z. Mao, Z. Han, V. V. Tuchin, and D. Zhu, J. Biophotonics **3**(1), 44–52 (2010).
[26] L. M. Oliveira, M. I. Carvalho, E. Nogueira, and V. V. Tuchin, Laser Phys. **23**(7), 075606 (2013).
[27] L. Oliveira, M. I. Carvalho, E. Nogueira, and V. V. Tuchin, J. Innov. Opt. Health Sci. **6**(2), 1350012 (2013).
[28] A. N. Bashkatov, E. A. Genina, Yu. P. Sinichkin, V. I. Kochubey, N. A. Lakodina, and V. V. Tuchin, Biophys. J. **85**(5), 3310–3318 (2003).
[29] X. Guo, G. Wu, H. Wei, X. Deng, H. Yang, Y. Ji, Y. He, Z. Guo, S. Xie, H. Zhong, Q. Zhao, and Z. Zhu, Photochem. & Photobiol. **88**, 311–316 (2012).
[30] D. G. Gardner and D. M. Shoback, Greenspan's Basic & Clinical Endocrinology (9th ed., NY: McGraw-Hill Medical, 2011).
[31] Diabetes Fact Sheet 312. WHO, October 2013; retrieved 10 July 2014 from http://www.who.int/mediacentre/factsheets/fs312/en/
[32] B. B. Tripathy (ed.) RSSDI Textbook of Diabetes Mellitus, (2nd ed., New Delhi: Jaypee Brothers Medical Publishers, 2012).
[33] The Top 10 Causes of Death Fact Sheet 310, World Health Organization (WHO), May 2014; retrieved 20 November 2014 from http://www.who.int/mediacentre/factsheets/fs310/en/
[34] N. Vigneshwaran, G. Bijukumar, N. Karmakar, S. Anand, and A. Misra, Spectrochimica Acta **A61** (1), 163–170 (2005).
[35] H. Ullah, A. Mariampillai, M. Ikram, and I. A. Vitkin, Laser Phys. **21**(11), 1962–1971 (2011).
[36] G. Purvinis, B. D. Cameron, and D. M. Altrogge, J. Diabetes Sci. Tech. **5**(2), 380–387 (2011).
[37] S. Firdous, M. Nawaz, M. Ahmed, S. Anwar, A. Rehman, R. Rashid, and A. Mahmood, Laser Phys. **22**(6), 1090–1094 (2012).
[38] J. M. Yuen, N. C. Shah, J. T. Walsh, Jr., M. R. Glucksberg, and R. P. Van Duyne, Anal. Chem. **82**(20), 8382– 8385 (2010).
[39] N. C. Dingari, I. Barman, G. P. Singh, J. W. Kang, R. R. Dasari, and M. S. Feld, Anal. Bioanal. Chem. **400**(9), 2871–2880 (2011).
[40] N. C. Dingari, I. Barman, J. W. Kang, C. R. Kong, R. R. Dasari, and M. S. Feld, J. Biomed. Opt. **16**(8), 087009 (2011).
[41] Y. Zhang, G. Wu, H. Wei, Z. Guo, H. Yang, Y. He, S. Xie, and Y. Liu, Biomed. Opt. Express **5**(4), 990–999 (2014).
[42] X. X. Guo, A. Mandelis, and B. Zinman, Biomed. Opt. Express **3**(11), 3012–3021 (2012).
[43] R. Y. He, H. J. Wei, H. M. Gu, Z. G. Zhu, Y. Q. Zhang, X. Guo, and T. Cai, J. Biomed. Opt. 17(10), 101513 (2012).
[44] M. A. Pleitez, T. Lieblein, A. Bauer, O. Hertzberg, H. von Lilienfeld-Toal, and W. Mäntele, Rev. Sci. Instr. **84**(8), 084901 (2013).
[45] Y. J. Heo and S. Takeuchi, Advanced Healthcare Materials **2**, 43–56 (2013).
[46] E. Selvin, M. W. Steffes, H. Zhu, K. Matsushita, L. Wagenknecht, J. Pankow, J. Coresh, and F. L. Brancati, N. Engl. J. Med. **362**, 800–811 (2010).
[47] J.-Y. Tseng, A. A. Ghazaryan, W. Lo, Y.-F. Chen, V. Hovhannisyan, S.-J. Chen, H.Y. Tan, and C.-Y. Dong, Biomed. Opt. Express **2**(2), 218–230 (2011).
[48] G. Mazarevica, T. Freivalds, and A. Jurka, J. Biomed. Opt. **7**(2), 244–247, (2002).
[49] J. Blackwell, K. M. Katika, L. Pilon, K. M. Dipple, S. R. Levin, A. Nouvong, J. Biomed. Opt. **13**(1), 014004 (2008).
[50] U. Kanska and J. Boratynski, Arch. Immunol. Therap. Exp. **50**, 61–66 (2002).
[51] M. Kreft, M. Luksic, T. M. Zorec, M. Prebil, and R. Zorec, Cell. Mol. Life Sci. **70**(8), 1483–1492 (2012).
[52] R. D. G. Leslie and David C. Robbins (eds.), Diabetes: Clinical Science in Practice (Cambridge University Press, 1995).
[53] J. Kinnunen, H. T. Kokkonen, V. Kovanen, M. Hauta-Kasari, P. Vahimaa, M. J. Lammi, J. Töyräs, and J. S. Jurvelinb, J. Biomed. Opt. **17**(9), 097003 (2012).
[54] G. T. Wondrak, M. J. Roberts, D. Cervantes-Laurean, M. K. Jacobson, and E. L. Jacobson, J. Invest. Dermatol. **121**(3), 578–586 (2003).
[55] E. L. Hull, M. N. Ediger, A. N. T. Unione, E. K. Deemer, M. L. Stroman, and J. W. Baynes, Opt. Express **12**(19), 4496–4510 (2004).
[56] B. Gopalkrishnapillai, V. Nadanathangam, N. Karmakar, S. Anand, and A. Misra, Diabetes **52**, 1041–1046 (2003).
[57] Y.-J. Hwang, J. Granelli, and J. Lyubovitsky, Analytical Chemistry **83**(1), 200–206 (2011).
[58] B.-M. Kim, J. Eichler, K. M. Reiser, A. M. Rubenchik, and L. B. Da Silva, Lasers Surg. Med. **27**, 329–335 (2000).

[59] A. Goldin, J. A. Beckman, A. M. Schmidt, and M. A. Creager, Circulation **114**, 597–605 (2006).
[60] O. S. Khalil, Diabetes Technology & Therapeutics **6**(5), 660–697 (2004).
[61] J. Nyström, B. Lindholm-Sethson, L. Stenberg, S. Ollmar, J. W. Eriksson and P. Geladi, Med. Biol. Eng. and Comput. **41**(3), 324–329 (2003).
[62] C. D. Brown, H. T. Davis, M. N. Ediger, C. M. Fleming, E. L. Hull, and M. Rohrscheib, Diabetes Technol. Ther. **7**(3) 456–466 (2005).
[63] H. A. Linares, C. W. Kischer, M. Dobrkovsky, and D. L. Larson, J. Invest. Dermatol. **59**(4), 323–331 (1972).
[64] M. E. Darvin, C. Sandhagen, W. Koecher, W. Sterry, J. Lademann, and M. C. Meinke, J. Biophoton. **5**(7), 550–558 (2012).
[65] M. Gniadecka, O. F. Nielsen, S. Wessel, M. Heidenheim, D. H. Christensen, and H. C. Wulf, J. Invest. Dermatol. **111**(6), 1129–1133 (1998).
[66] S. H. Chung, A. E. Cerussi, S. I. Merritt, J. Ruth, and B. J. Tromberg, Phys Med. Biol. **55**(13), 3753–3765 (2010).
[67] K. A. Martin, J. Soc. Cosm. Chem. **44**, 249–261 (1993).
[68] A. Hidenobu and E. Mariko, Appl. Spectrosc. **58**, 1439–1446 (2004).
[69] C. Li, J. Jiang, and K. Xu, J. Innov. Opt. Health Sci. **6**(1), 1350005-1–9 (2013).
[70] B. Schulz, D. Chan, J. Backstrom, and M. Rubhausen, Thin Solid Films **455–456**, 731–734 (2004).
[71] O. F. Nielsen, M. Bilde, and M. Frosch, Spectroscopy: Intern. J. **27**(5–6), 565–569 (2012).
[72] P. J. Caspers, G. W. Lucassen, and G. J. Puppels, Biophys J. **85**(1), 572–580 (2003).
[73] N. Nakagawa, M. Matsumoto, and S. Sakai, Skin Res. Technol. **16**, 137–141 (2010).
[74] P. Ballard, D. E. Leahy, and M. Rowland, Pharm. Res. **17**(6), 660–663 (2000).
[75] K. Martin, Appl. Spectrosc. **52**(7), 1001–1007 (1998).
[76] Y.-A. Woo, J.-W. Ahn, I.-K. Chun, and H.-J. Kim, Anal. Chem. **73**, 4964–4971 (2001).
[77] A. Rohilla and S. Ali, Intern. J. Res. Pharm. Biomed. Sci. **3**(2), 819–823 (2012).
[78] J. R. Garrett, J. Ekström, and L. C. Anderson (eds.), Frontiers of Oral Biology: Glandular Mechanisms of Salivary Secretion Vol. 10 (1998).
[79] A. N. Bashkatov, E. A. Genina, and V. V. Tuchin, in: V. V. Tuchin (ed.), Handbook of Optical Sensing of Glucose in Biological Fluids and Tissues, (Taylor & Francis Group LLC, CRC Press, 2009), pp. 587–621.
[80] D. W. Leonard and K. M. Meek, Biophys. J. **72**(3), 1382–1387 (1997).
[81] A. N. Bashkatov, E. A. Genina, V. V. Tuchin, J. Innov. Opt. Health Sci. **4**(1), 9–38 (2011).
[82] J. S. Maier, S. A. Walker, S. Fantini, M. A. Franceschini, and E. Gratton, Opt. Lett. **19**(24), 2062–2064 (1994).
[83] M. Kohl, M. Essenpreis, and M. Cope, Phys. Med. Biol. **40**, 1267–1287 (1995).
[84] J. M. Schmitt and G. Kumar, Appl. Opt. **37**(13), 2788–2797 (1998).
[85] C. F. Bohren and D. R. Huffman, Absorption and scattering of light by small particles (John Willey & Sons Inc., New York, 1983).
[86] Y. Huang and K. M. Meek, Biophysical J. **77**, 1655–1665 (1999).
[87] W. Schneider, T. Bortfeld, and W. Schlegel, Phys. Med. Biol. **45**, 459–478 (2000).
[88] A. N. Bashkatov, E. A. Genina, I. V. Korovina, V. I. Kochubey, Yu. P. Sinichkin, and V. V. Tuchin, Proc. SPIE **4224**, 300–311 (2000).
[89] W. H. Press, S. A. Tuekolsky, W. T. Vettering, and B. P. Flannery, Numerical Recipes in C: The Art of Scientific Computing (Cambridge University Press, Cambridge, New York, 1992).
[90] T. Yu, X. Wen, V. V. Tuchin, Q. Luo, and D. Zhu, Quantitative analysis of dehydration in porcine skin for assessing mechanism of optical clearing, J. Biomed. Opt. **16**(9), 095002 (2011).
[91] A. Kotyk and K. Janacek, Membrane Transport: An Interdisciplinary Approach, Plenum Press, New-York (1977).
[92] A. N. Bashkatov, E. A. Genina, V. I. Kochubey, and V. V. Tuchin, J. Physics D: Appl. Phys. **38**(15), 2543–2555 (2005).
[93] W. Hanna, D. Friesen, C. Bombardier, D. Gladman, and A. Hanna, J. Am. Acad. Dermatol. **16**, 546–553 (1987).
[94] S. Tanaka, G. Avigad, B. Brodsky, and E. F. Eikenberry, J. Mol. Biol. **203**, 495–505 (1988).
[95] H. N. Mayrovitz, A. McClymont, and N. Pandya, Diabetes Technol. Therap. **15**(1), 60–65 (2013).
[96] D. R. Lide (ed.), Handbook of Chemistry and Physics (84th Edition, CRC Press, 2003).
[97] A. A. Gurjarpadhye, W. C. Vogt, Y. Liu, and C. G. Rylander, Intern. J. Biomed. Imaging **2011**, 817250-1–8 (2011).
[98] V. Hovhannisyan, P.-S. Hu, S.-J. Chen, C.-S. Kim, and C.-Y. Dong, J. Biomed. Opt. **18**(4), 046004-1–8 (2013).
[99] N. Vogler, S. Heuke, D. Akimov, I. Latka, F. Kluschke, H.-J. Rowert-Huber, J. Lademann, B. Dietzek, and J. Popp, Proc. SPIE **8427**, 842710 (2012).
[100] R. Grüner, I. Latka, J. Lademann, B. Dietzek, and J. Popp, Laser Phys. Lett. **10**(6), 065605 (2013).
[101] H.-M. Raabe, H. Molsen, S.-M. Mlinaric, Y. Acil, G. H. G. Sinnecker, H. Notbohm, K. Kruse and P. K. Muller, Biochem. J. **319**, 699–704 (1996).
[102] O. S. Zhernovaya, A. N. Bashkatov, E. A. Genina, V. V. Tuchin, I. V. Meglinski, D. Yu. Churmakov and L. J. Ritchie, Proc. of SPIE **6535**, 65351C (2007).
[103] P. J. Higgins and H. F. Bunn, J. Biol. Chem. **256**(10), 5204–5208 (1981).
[104] S. F. Diniz, F. P. L. G. Amorim, F. F. Cavalcante-Neto, A. L. Bocca, A. C. Batista, G. E. P. M. Simm, and T. A. Silva, Braz J Med Biol Res **41**(5), 373–379 (2008).
[105] J. Wang, Y. Zhang, P. Li, Q. Luo, and D. Zhu, IEEE J. Select. Tops Quant. Electr. **20**(2), 6801112-1–12 (2014).
[106] J. Wang, R. Shi, and D. Zhu, J. Biomed. Opt. **18**(6), 061209-1–6 (2013).